Non-cell-autonomous role for *Cripto* in axial midline formation during vertebrate embryogenesis

Jianhua Chu[1], Jixiang Ding[1,*], Katherine Jeays-Ward[2], Sandy M. Price[1], Marysia Placzek[2] and Michael M. Shen[1,†]

[1]Center for Advanced Biotechnology and Medicine and Departments of Pediatrics, UMDNJ-Robert Wood Johnson Medical School, Piscataway, NJ 08854, USA
[2]Centre for Developmental and Biomedical Genetics, Department of Biomedical Science, University of Sheffield, Sheffield S10 2TN, UK
*Present address: Department of Molecular, Cellular, and Craniofacial Biology, Birth Defects Center, University of Louisville Health Sciences Center, Louisville, KY 40202 USA
†Author for correspondence (e-mail: mshen@cabm.rutgers.edu)

Development 132, 5539-5551
Published by The Company of Biologists 2005
doi:10.1242/dev.02157

Accepted 11 October 2005

Summary

Several membrane-associated proteins are known to modulate the activity and range of potent morphogenetic signals during development. In particular, members of the *EGF-CFC* family encode glycosyl-phosphatidylinositol (GPI)-linked proteins that are essential for activity of the transforming growth factor β (TGFβ) ligand Nodal, a factor that plays a central role in establishing the vertebrate body plan. Genetic and biochemical studies have indicated that EGF-CFC proteins function as cell-autonomous co-receptors for Nodal; by contrast, cell culture data have suggested that the mammalian EGF-CFC protein Cripto can act as a secreted signaling factor. Here we show that Cripto acts non-cell-autonomously during axial mesendoderm formation in the mouse embryo and may possess intercellular signaling activity in vivo. Phenotypic analysis of hypomorphic mutants demonstrates that *Cripto* is essential for formation of the notochordal plate, prechordal mesoderm and foregut endoderm during gastrulation. Remarkably, *Cripto* null mutant cells readily contribute to these tissues in chimeras, indicating non-cell-autonomy. Consistent with these loss-of-function analyses, gain-of-function experiments in chick embryos show that exposure of node/head process mesoderm to soluble Cripto protein results in alterations in cell fates toward anterior mesendoderm, in a manner that is dependent on Nodal signaling. Taken together, our findings support a model in which Cripto can function in trans as an intercellular mediator of Nodal signaling activity.

Key words: EGF-CFC proteins, Axial mesendoderm, Chimera analysis, Non-cell-autonomy, Co-receptor, Nodal signaling, Mouse

Introduction

The emergence of axial mesendoderm from the anterior primitive streak is a crucial event during vertebrate gastrulation that requires precise control of cell fate determination in a limited spatial and temporal context. The recruitment and differentiation of axial mesendoderm progenitors result in formation of the node, prechordal plate, notochordal plate and a population of anterior definitive endoderm that contributes to the foregut (Kinder et al., 2001; Tam and Beddington, 1987). Previous studies have established that several components of the Nodal signaling pathway are essential for axial mesendoderm formation (e.g. Chu et al., 2004; Dunn et al., 2004; Hoodless et al., 2001; Lowe et al., 2001; Norris et al., 2002; Vincent et al., 2003; Yamamoto et al., 2001). Nodal signaling is also believed to play a central role in specifying axial mesoderm subtypes, as differential levels of Nodal activity can specify prechordal mesoderm versus notochord during gastrulation (Agius et al., 2000; Gritsman et al., 2000; Lowe et al., 2001; Norris and Robertson, 1999; Thisse et al., 2000; Vincent et al., 2003). Furthermore, high levels of Nodal pathway activity are also essential for formation of the definitive endoderm (reviewed by Ober et al., 2003; Tam et al., 2003).

Molecular genetic studies in several vertebrate systems have identified EGF-CFC proteins as essential components of the Nodal signaling pathway, and have demonstrated their ability to act in cis as co-receptors for Nodal ligands (Gritsman et al., 1999; Kumar et al., 2001; Reissmann et al., 2001; Yan et al., 2002; Yeo and Whitman, 2001). EGF-CFC proteins are small extracellular proteins that contain a divergent epidermal growth factor (EGF) motif and a novel conserved cysteine-rich domain (termed the CFC motif) (reviewed by Shen and Schier, 2000), and they are attached to the cell membrane through a glycosyl-phosphatidylinositol (GPI) linkage (Minchiotti et al., 2000). Two *EGF-CFC* genes, *Cripto* (*Tdgf1*) and *Cryptic* (*Cfc1* – Mouse Genome Informatics), have been identified in mammals; other family members include chick *Cripto,* frog *FRL-1* and zebrafish *one-eyed pinhead* (*oep*). In the case of *oep,* cell transplantation experiments have shown its cell-autonomy in prechordal plate, floor plate, and endoderm (Gritsman et al., 1999; Schier et al., 1997; Strahle et al., 1997). These data, together with the absence of phenotypic

consequences following *oep* overexpression in zebrafish embryos (Zhang et al., 1998), are consistent with a strict role for Oep as a cis-acting co-receptor for Nodal.

Zygotic *oep* mutants lose axial mesendoderm and display associated ventral midline and forebrain defects (Schier et al., 1997). Despite a relatively low overall level of sequence conservation, all *EGF-CFC* family members appear to have functionally similar activities in assays for phenotypic rescue of *oep* mutants (Zhang et al., 1998). However, it has been unclear to date whether, like Oep, mammalian EGF-CFC proteins are required in axial midline formation and forebrain patterning, and whether they function as cis-acting co-receptors for Nodal in this context. Intriguingly, by contrast with Oep, studies of Cripto function have raised the possibility that it can function as a secreted trans-acting signaling factor (Bianco et al., 2003; Kannan et al., 1997; Minchiotti et al., 2001; Parisi et al., 2003; Yan et al., 2002). Furthermore, a previous low-resolution chimera analysis has suggested potential non-cell-autonomy for *Cripto* (Xu et al., 1999), although the absence of cell-marking in this experiment precluded analysis of specific requirements for *Cripto* function during embryogenesis.

In the studies described below, we show that *Cripto,* like other Nodal pathway components, is required for axial mesendoderm and definitive endoderm formation in mouse embryogenesis. However, we find that this requirement for *Cripto* is non-cell-autonomous, and provide evidence that Cripto can act as a soluble trans-acting factor in vivo. Complementary gain-of-function approaches in chick embryos reveal effects of exogenous soluble Cripto protein on differentiation of chick node/head process mesoderm cells, suppressing posterior axial mesoderm fates and promoting anterior mesendodermal fates. Our findings potentially resolve long-standing discrepancies concerning the mechanisms of Cripto function, and suggest that a GPI-linked protein can act as a trans-acting signal.

Materials and methods

Gene targeting

To generate the *Cripto*^{3loxP} targeting construct, a 5.5 kb genomic *Bam*HI fragment containing exon 6 was cloned into the 3′ multiple cloning site of p*loxP*NT (Shalaby et al., 1995), followed by cloning of a 5′ arm corresponding to a 3.1 kb *Hin*dIII-*Bam*HI partial digest fragment containing exons 1-5; a *loxP* site was inserted into the *Bam*HI site in intron 2. TC1 embryonic stem (ES) cell clones were screened for homologous recombination by Southern blotting with both 5′ and 3′ probes, with positive clones obtained at an efficiency of 25% (n=20).

We used the *EIIa-Cre* transgenic line to obtain both partial and complete deletions in vivo, taking advantage of the low Cre activity in the germline of *EIIa-Cre* males (Xu et al., 2001). We obtained all three possible deletion products with approximately equal frequency in the progeny of C57BL/6 wild-type females × *EIIa-Cre; Cripto*$^{3loxP/+}$ males, including the desired *Cripto*^{del} and *Cripto*^{flox} alleles. (Formal allele names are as follows: *Cripto*^{lacZ}=*Cripto*^{tm1Mms}; *Cripto*^{3loxP}=*Cripto*^{tm2Mms}; *Cripto*^{del}=*Cripto*$^{tm2.1Mms}$; *Cripto*^{flox}=*Cripto*$^{tm2.2Mms}$). PCR primers used for genotyping were: *Cripto*^{3loxP} (forward) 5′-CCT CCC AAG TTC ACT ACC AAA TCT-3′, (reverse) 5′-TCC CCA CCA TCC ACC ACC AAG TAG-3′; *Cripto*^{del} (forward) 5′-AGC CAT CTC ACC AGC CTT CA-3′, (reverse) 5′-CAT CTG GGA CAT GCC CAC TA-3′; *Cripto*^{lacZ} (forward) 5′-CCA TCC CCT GCC CGT CTA CAC G-3′, (reverse) 5′-GTC ACG CAA CTC GCC GCA CAT-3′.

Histology, in situ hybridization, and β-galactosidase staining

Whole-mount in situ hybridization and β-galactosidase staining were performed as described (Ding et al., 1998). Genotypes of 6.5 days-post-coitum (dpc) embryos were determined by PCR using genomic DNA from cultured extraplacental cone (Ang and Rossant, 1994); for 7.5 dpc embryos and older, extra-embryonic tissues following in situ hybridization were lysed for DNA extraction and PCR. Following whole-mount in situ hybridization, embryos were embedded in OCT and 6 μm cryosections were counterstained with Methyl Green, or left unstained. Histological analysis was performed by hematoxylin and eosin staining of paraffin sections of embryos fixed in 10% formalin. Mouse probes for in situ hybridization were: *Cer1* (Belo et al., 1997); *Cripto* (Ding et al., 1998); *En1* (Davis and Joyner, 1988); *Fgf8* (Crossley and Martin, 1995); *Foxa2* (Ang and Rossant, 1994); *Gsc* (Belo et al., 1997); *Hex* (*Hhex*) (Thomas et al., 1998); *Shh* (Echelard et al., 1993); and *Six3* (Oliver et al., 1995). Chick probes were *Gsc* (Hume and Dodd, 1993) and *Hex* (Crompton et al., 1992).

Chimera analysis

Chimeras were generated by morula aggregation (Nagy et al., 2003), using 4-8 cell embryos from pregnant C57BL/6 wild-type mice and from a *Rosa26/Rosa26; Cripto*$^{null/+}$ × *Cripto*$^{lacZ/+}$ cross (here we refer to the *Gt(ROSA)26Sor* gene-trap allele as *Rosa26*). Embryos were recovered at 7.5-9.5 dpc, and genotypes determined by PCR analysis of DNA extracted from extra-embryonic tissues. Whole-mount embryos were stained for β-galactosidase activity, and cryosections were counterstained with Nuclear Fast Red (Vector Laboratories). In a second method of chimera analysis, marked ES cell lines were established from blastocysts obtained by a *Rosa26/Rosa26; Cripto*$^{del/+}$ × *Cripto*$^{lacZ/+}$ cross, using standard methods (Nagy et al., 2003). The resulting ES colonies were genotyped by PCR, and a *Rosa26/+; Cripto*$^{lacZ/del}$ cell line and a *Rosa26/+; Cripto*$^{lacZ/+}$ line were established. Chimeras were generated by injecting approximately 5-10 ES cells into C57BL/6 blastocysts.

Chick explant cultures, in-ovo operations and immunofluorescence

Embryos and explants were assayed according to standard techniques (Placzek et al., 1993; Placzek et al., 1990). For explant culture experiments, posterior head process mesoderm or Hensen's node explants were grown for 20 hours in Optimem (Invitrogen) containing 2% fetal calf serum, 1% penicillin/streptomycin, and 1% L-glutamine, either alone or with addition of 10-fold concentrated 293T culture supernatants. 293T cells were either untransfected or transfected with full-length mouse *Cripto*, which results in production of active Cripto protein in conditioned medium (Minchiotti et al., 2000; Yan et al., 2002). The small molecule inhibitor SB-431542 was used as described previously (Inman et al., 2002). For in-ovo experiments, beads were grafted at Hamburger-Hamilton (HH) stage 3-4 and embryos developed until HH stage 8-9. Explants and embryos were fixed in 4% paraformaldehyde for 2 hours and embedded in OCT for cryosectioning. Sections were processed for immunofluorescence detection using the 3B9 monoclonal antibody [1:10 dilution from culture supernatant (Placzek et al., 1990)] or the Shh monoclonal antibody (Ericson et al., 1996) and a Cy3-labeled anti-mouse secondary antibody (Jackson ImmunoResearch; 1:200 dilution), as described previously (Placzek et al., 1993).

Quantitative RT-PCR

Real-time quantitative RT-PCR was performed using the ABI Prism 7700 sequence detection system (Applied Biosystems). RNA was standardized using β-actin amplification as an internal control. Primers used were: *Gsc* (forward) 5′-AAA AGA CGG CAC CGG ACT ATC-3′, (reverse) 5′-TCG TTT CCT GGA AGA GGT TTT C-3′, and the probe 5′-CAC TGA CGA GCA GCT CGA AGC GC-3′ (labeled with the reporter dye FAM on the 5′ nucleotide and the

quenching dye TAMRA on the 3′ nucleotide). *Fgf10* (forward) 5′-ATG ACC TCG GCC AGG ACA T-3′, (reverse) 5′-TGA TTG TAG CTC CGC ACG TG-3′, and probe 5′-CTG TCC CCG GAG GCC ACC AA-3′ labeled with the reporter Yakima Yellow on the 5′ nucleotide and the quenching dye Eclipse Dark Quencher on the 3′ nucleotide. β-actin (forward) 5′-GGT CAT CAC CAT TGG CAA TG-3′, (reverse) 5′-CCC AAG AAA GAT GGC TGG AA-3′ and the fluorogenic probe 5′-TTC AGG TGC CCC GAG GCC CT-3′ labeled with the reporter dye Yakima Yellow on the 5′ nucleotide and the quenching dye Eclipse Dark Quencher on the 3′ nucleotide. Probes were supplied by Eurogentec. Relative quantification of *Gsc* and *Fgf10* mRNA was calculated using the standard curve method.

Results

Expression of *Cripto* in precursors of axial mesoderm and anterior definitive endoderm

We previously described the expression pattern of *Cripto* in the pre-gastrulation epiblast and in the primitive streak and nascent mesoderm (Ding et al., 1998). At later stages of gastrulation, we observe *Cripto* expression in the embryonic mesoderm and node, as well as in the axial mesendoderm (Fig. 1A-C). However, this expression of *Cripto* disappears during neural plate stages (data not shown).

To determine the cell types that derive from this transient expression of *Cripto*, we took advantage of the $Cripto^{lacZ}$ null allele, in which the *lacZ* reporter gene is under the control of the *Cripto* promoter (Ding et al., 1998). This knock-in allele recapitulates the pattern of endogenous *Cripto* expression, except for a temporal delay that probably corresponds to the perdurance of β-galactosidase (Ding et al., 1998). In $Cripto^{lacZ/+}$ heterozygotes at late neural plate stages, we found β-galactosidase staining throughout the mesoderm and definitive endoderm, with strongest staining in the axial mesendoderm (Fig. 1D,E). Taken together, these data indicate that *Cripto*-expressing cells give rise to axial mesendoderm and anterior definitive endoderm.

Generation of a hypomorphic allele of *Cripto*

Cripto null mutants display early embryonic lethality due to a failure in anterior-posterior axis positioning before gastrulation (Ding et al., 1998). Therefore, to investigate subsequent functions of *Cripto* in embryogenesis, we have generated novel hypomorphic (partial loss-of-function), conditional, and null alleles for *Cripto* (Fig. 1F-H). In our targeting strategy, a '3-*loxP*' construct containing a 'floxed' (flanked by *loxP* sites) *PGK-neo* selection cassette was inserted at the *Cripto* locus. Following germline transmission of this allele, mice carrying this $Cripto^{3loxP}$ allele were crossed with *Ella-Cre* transgenic mice to produce all three possible derivatives from Cre-loxP mediated recombination (Xu et al., 2001). This strategy resulted in the generation of a new null allele corresponding to the deletion of exons 3, 4 and 5 ($Cripto^{del}$) (Fig. 1F), as well as a conditional floxed allele ($Cripto^{flox}$) (data not shown). Both homozygous $Cripto^{del}$ and heteroallelic $Cripto^{lacZ/del}$ embryos displayed a phenotype identical to that of $Cripto^{lacZ}$ homozygotes (data not shown).

As the intronic insertion of selection cassettes with strong transcription termination sequences frequently leads to the generation of a hypomorphic allele (Meyers et al., 1998), we performed genetic crosses to determine whether the $Cripto^{3loxP}$ allele might be hypomorphic. Although homozygous $Cripto^{3loxP}/Cripto^{3loxP}$ mice can be recovered as adults at Mendelian ratios (Table 1A), we observed that progeny from crosses of $Cripto^{3loxP}$/+ and $Cripto^{lacZ}$/+ mice were significantly under-represented for the $Cripto^{3loxP/lacZ}$ genotype (Table 1B). The surviving mice with this genotype can reach adulthood and breed successfully; gross and histological examination of these mice has not yet revealed any phenotypic abnormality (J.C. and M.M.S., unpublished). Because $Cripto^{3loxP/del}$ embryos displayed an identical phenotype to $Cripto^{3loxP/lacZ}$ embryos (data not shown), we refer to both $Cripto^{3loxP/lacZ}$ and $Cripto^{3loxP/del}$ embryos as having a $Cripto^{3loxP/null}$ genotype.

Table 1. Genotype analysis of crosses with $Cripto^{3loxP}$ mice

(A) Progeny from $Cripto^{3loxP/+} \times Cripto^{3loxP/+}$

	$Cripto^{3loxP/3loxP}$	$Cripto^{3loxP/+}$	$Cripto^{+/+}$	Total
Four weeks post-natal	20 (30%)	33 (50%)	12 (18%)	66

(B) Progeny from $Cripto^{3loxP/+} \times Cripto^{lacZ/+}$

	$Cripto^{3loxP/lacZ}$	$Cripto^{3loxP/+}$	$Cripto^{lacZ/+}$	$Cripto^{+/+}$	Total
7.5 dpc	41 (24%)	36 (22%)	36 (22%)	54 (32%)	167
Four weeks post-natal	5 (8%)*	16 (24%)	25 (38%)	20 (30%)	66

*Significantly under-represented ($P<0.01$).

Reduction of *Cripto* activity results in a holoprosencephaly phenotype

Morphological and histological examination of $Cripto^{3loxP/null}$ embryos at 8.25-9.5 dpc showed that approximately 56% (n=52) displayed a broad spectrum of phenotypes that recapitulate many of the characteristic features of human holoprosencephaly (Fig. 2). The most severely affected embryos showed anterior truncations as well as fusions of anterior somites across the midline, indicating the absence of notochord (Fig. 2A-C). Less-affected embryos displayed anterior-restricted phenotypes, including cyclopia (Fig. 2D-G) and variable forebrain and midbrain reductions at 9.0-11.5 dpc (Fig. 2D-I). Finally, histological analyses of the brains of severely affected $Cripto^{3loxP/null}$ embryos showed a single prosencephalic vesicle (Fig. 2J,K), consistent with the absence of ventral patterning signals from the axial mesendoderm.

Next, we examined the expression of specific tissue markers in severely affected $Cripto^{3loxP/null}$ embryos to ascertain the basis for these phenotypic defects. *Sonic hedgehog* (*Shh*) is expressed in ventral midline structures and gut endoderm at 8.25 dpc, but was often greatly reduced or absent in $Cripto^{3loxP/null}$ embryos (71%, n=7) (Fig. 3A). Similarly, *Hex* is a marker of anterior definitive endoderm at 7.5 dpc, but was often undetectable in $Cripto^{3loxP/null}$ mutants (40%, n=15) (Fig. 3B); by contrast, *Hex* expression in the anterior visceral endoderm at 6.5 dpc was unaffected (n=5; data not shown). Analyses of neural markers revealed that severely affected $Cripto^{3loxP/null}$ embryos retain expression of the midbrain-hindbrain marker *En1* (n=4) (Fig. 3C). However, $Cripto^{3loxP/null}$ embryos often displayed truncation of the rostral forebrain, as shown by loss of anterior expression for *Six3* (67%, n=9) and *Fgf8* (63%, n=8) (Fig. 3D-F). The loss of *Hex* expression, in particular, suggests that the forebrain defects may represent a

secondary consequence of the loss of axial mesendoderm derivatives, notably the anterior definitive endoderm and prechordal plate (reviewed by Kiecker and Niehrs, 2001; Wilson and Houart, 2004).

Consistent with this interpretation, histological and marker analyses of *Cripto*$^{3loxP/null}$ embryos during gastrulation stages demonstrated severe defects in the formation of axial mesendoderm and definitive endoderm. In wild-type embryos, the prechordal plate is evident from the apposition of axial mesendoderm to anterior ectoderm at the midline (Fig. 2L), whereas an intact prechordal plate did not form in *Cripto*$^{3loxP/null}$ mutants (Fig. 2M,N). At head-fold stages, *Shh* is expressed in the node, notochordal plate and prechordal plate, but in *Cripto*$^{3loxP/null}$ mutants was either absent or occasionally observed in scattered patches of mesodermal cells that were displaced from the midline (53%, *n*=19) (Fig. 4A-D). Similar results were obtained with the axial midline markers *Foxa2* (HNF3β) (36%, *n*=14) (Fig. 4E-H) and chordin (*Chrd*, 67%, *n*=10/15) (data not shown). Expression of goosecoid (*Gsc*) marks prechordal plate, adjacent midline neuroectoderm and foregut endoderm, but was abolished in approximately half of *Cripto*$^{3loxP/null}$ mutants (50%, *n*=6) (Fig. 4I-L). Finally, expression of cerberus 1 homolog (*Cer1*) showed the nearly complete loss of definitive endoderm in strongly affected *Cripto*$^{3loxP/null}$ embryos (50%, *n*=4) (Fig. 4M-P), consistent with the results with *Hex* (Fig. 3B).

Chimera analysis demonstrates non-cell-autonomy of *Cripto* in the axial mesendoderm

To determine whether the requirement for *Cripto* in axial mesendoderm and definitive endoderm is cell-autonomous or non-cell-autonomous, we performed genetic mosaic analysis using two distinct and complementary methods to generate marked chimeras of wild-type and *Cripto* null mutant cells. In the first approach, we generated chimeric embryos using morula aggregation between wild-type embryos and morulas generated from a cross between mice carrying two different *Cripto* null mutant alleles (Fig.

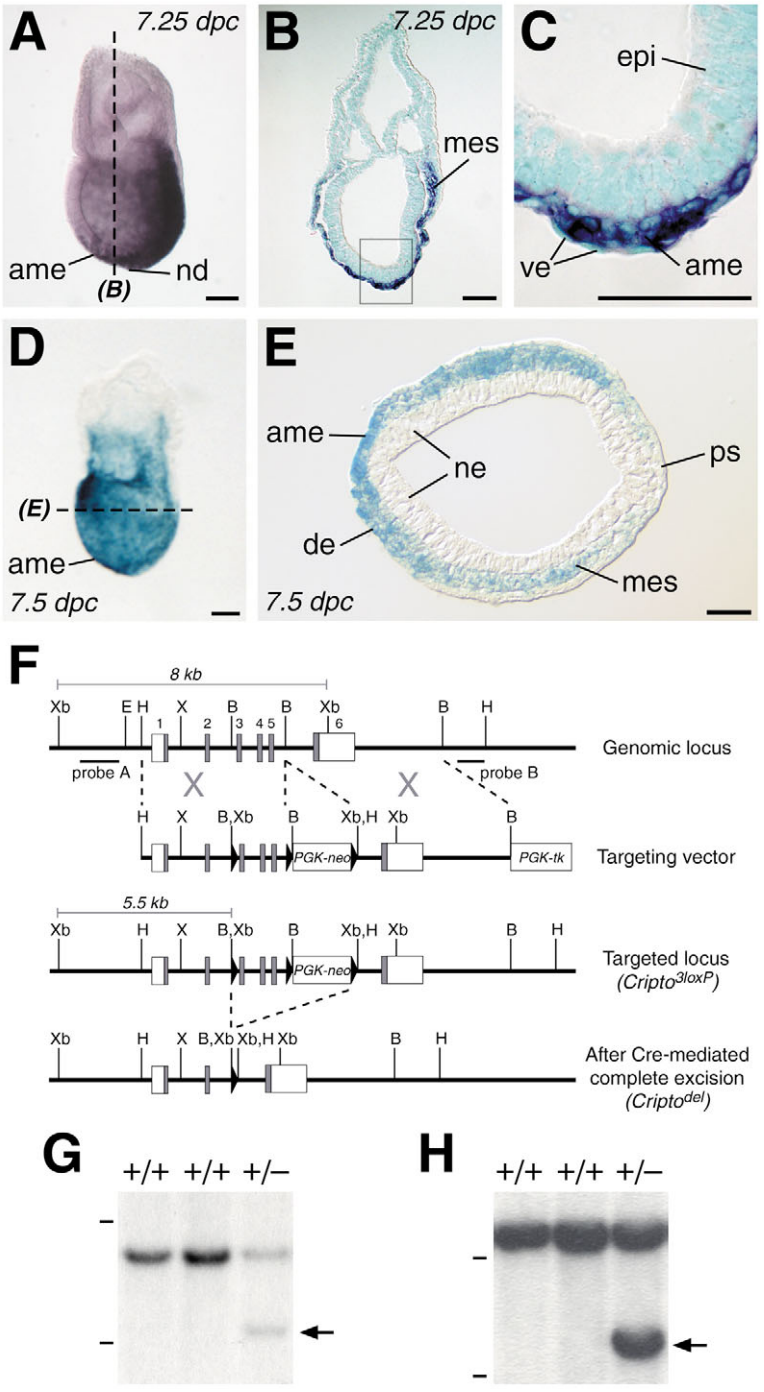

Fig. 1. *Cripto* expression and gene targeting. (A-C) Expression of *Cripto* in nascent mesoderm, node and axial mesendoderm of a wild-type late-streak stage embryo; frontal section in B is counterstained with Methyl Green. (C) High-power view of boxed region in B shows expression in midline mesendodermal cells, but not in epiblast or visceral endoderm cells being displaced during gastrulation. (D,E) Widespread β-galactosidase staining in a heterozygous *Cripto*$^{lacZ/+}$ embryo at the neural plate (late allantoic bud) stage; transverse section in E shows staining in the nascent mesoderm and definitive endoderm, with most intense staining in the axial mesendoderm; no expression is detected in the primitive streak or neuroectoderm. (F-H) Generation of hypomorphic and null alleles of *Cripto*. (F) The targeting strategy for the *Cripto*^{3loxP} allele inserts a floxed *PGK-neo* cassette into the intron between *Cripto* exons 5 and 6. Following germline transmission, the *PGK-neo* cassette was deleted by crossing the *Cripto*$^{3loxP/+}$ mice with *EIIa-Cre* transgenic mice; complete excision results in the null allele *Cripto*^{del}. (G) Southern blot detection of the targeted allele in ES genomic DNA digested with *Xba*I. An 8 kb fragment is detected by probe A for the wild-type allele, and a 5.5 kb fragment (arrow) is detected for the *Cripto*^{3loxP} allele. (H) Southern blot detection of the targeted allele using probe B in ES genomic DNA digested with *Hin*dIII; 11 kb (wild-type) and 6.8 kb (targeted) fragments are detected. Positions of molecular standards at 10 and 5 kb are indicated. Scale bars: 100 μm in A-D; 50 μm in E. ame, axial mesendoderm; B, *Bam*HI; de, definitive endoderm; E, *Eco*RI; epi, epiblast; H, *Hin*dIII; mes, nascent mesoderm; nd, node; ne, neuroectoderm; ps, primitive streak; ve, visceral endoderm; X, *Xho*I; Xb, *Xba*I.

5A) (Rivera-Perez et al., 1999). In this scheme, chimeric embryos are genotyped retrospectively using visceral yolk sac DNA, while the use of two *Cripto* alleles that can be distinguished by PCR allows for the unambiguous detection of chimeras containing null mutant cells (Fig. 5B). Cells derived from progeny of the *Cripto* heterozygote cross are marked by the *Rosa26* gene-trap allele, which ubiquitously expresses β-galactosidase activity (Friedrich and Soriano, 1991; Zambrowicz et al., 1997). One principal advantage of this approach is that control chimeras are generated together with the desired mutant chimeras, thereby reducing any potential experimental bias in their analysis.

Using morula aggregation, we generated 31 total chimeras, including 9 *Cripto*$^{lacZ/del}$↔ +/+ chimeras, which were examined at head-fold stages or at 9.5 dpc. These embryos were sectioned and assessed for their extent of chimerism as measured by the percentage of β-galactosidase stained cells, corresponding to expression of the *Rosa26* marker (Table 2). In control chimeras (*Cripto*$^{+/+}$↔ +/+, *Cripto*$^{lacZ/+}$ +/+, or *Cripto*$^{del/+}$↔ +/+), the β-galactosidase-stained cells were equally distributed among all germ layers and tissue types (data not shown). Unexpectedly, we found that low-grade (<50% contribution of marked cells) and medium-grade (~50% contribution) *Cripto*$^{lacZ/del}$↔ +/+ chimeras were phenotypically wild type (Fig. 6A-J; data not shown). In medium-grade *Cripto*$^{lacZ/del}$↔ +/+ chimeras at head-fold stages, there was no discernible bias in contribution of *Cripto* null mutant (blue) cells to all three germ layers (Fig. 6B,D). In particular, β-galactosidase-staining cells could be found in the notochordal plate and prechordal plate, which appeared morphologically normal (Fig. 6C,E). At 9.5 dpc, *Cripto*$^{lacZ/del}$↔ +/+ chimeras were also phenotypically wild type, with abundant contribution of marked cells to notochord, floor plate and foregut endoderm (Fig. 6F-J). Surprisingly, only a proportion of higher-grade (>50% contribution) *Cripto*$^{lacZ/del}$↔

Table 2. Distribution of *Cripto* chimera genotypes and grades from morula aggregations

Chimera genotype	<25%	25-50%	50-75%	>75%	Total
Cripto$^{+/+}$↔ +/+	2	1	1	3	7
Cripto$^{lacZ/+}$↔ +/+	2	1	3	3	9
Cripto$^{del/+}$↔ +/+	0	2	4	0	6
Cripto$^{lacZ/del}$↔ +/+	1	2	3 (1*)	3 (2*)	9
Total	5	6	11	9	31

*Embryos displaying a hypomorphic *Cripto* phenotype.

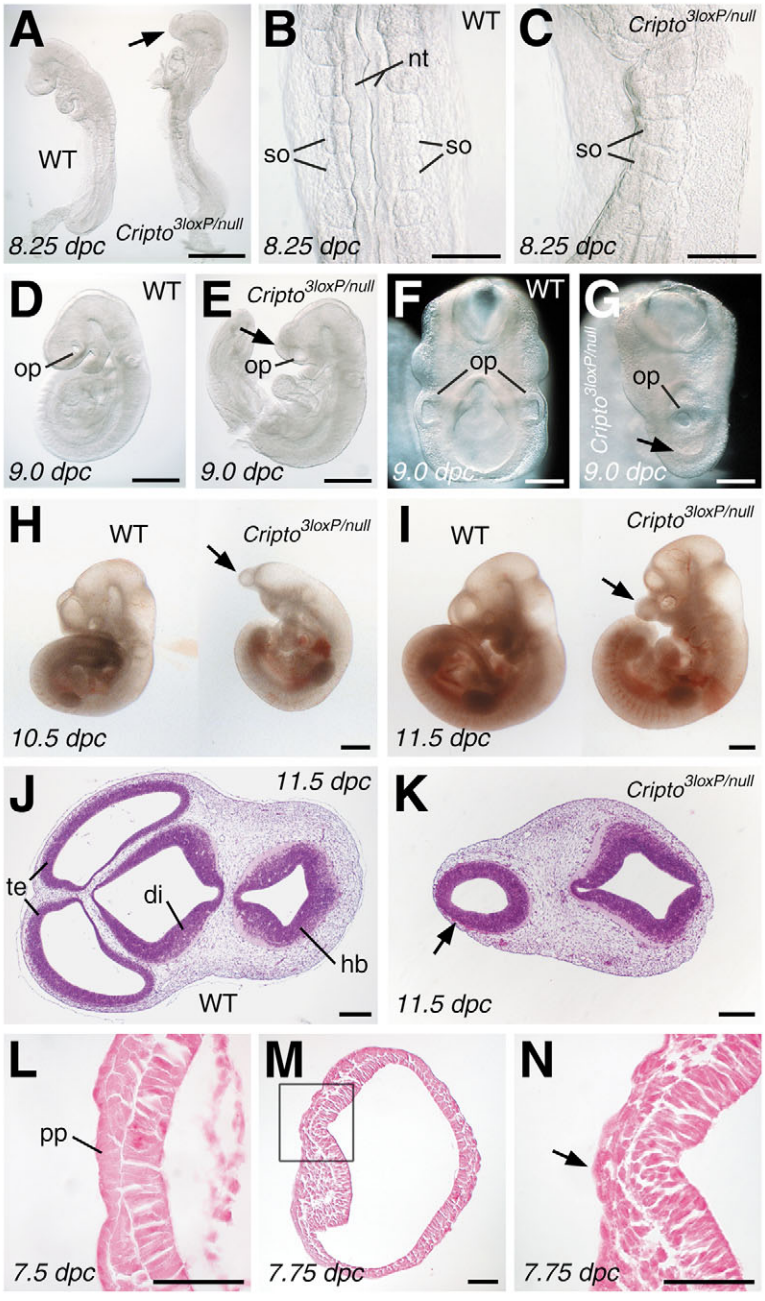

Fig. 2. Holoprosencephaly phenotypes in *Cripto*$^{3loxP/null}$ embryos. (A-C) Lateral (A) and ventral (B,C) views of wild-type and *Cripto*$^{3loxP/null}$ embryos at 8.25 dpc, showing anterior truncation (arrow in A) and fusion of somite pairs across the midline (C). (D-G) Lateral (D,E) and coronal (F,G) views of wild-type and *Cripto*$^{3loxP/null}$ embryos at 9.0 dpc, showing forebrain reduction (arrows in E,G) and fusion of optic vesicles. (H) Lateral view of wild-type and *Cripto*$^{3loxP/null}$ embryos at 10.5 dpc, showing greatly reduced forebrain and midbrain (arrow) in the mutant. (I) Lateral views of 11.5 dpc wild-type and *Cripto*$^{3loxP/null}$ embryos, with reduced telencephalon (arrow) in the mutant. (J,K) Coronal sections of 11.5 dpc wild-type (J) and *Cripto*$^{3loxP/null}$ mutant (K) littermates, stained with hematoxylin and eosin. While the wild-type embryo has distinct telencephalic and diencephalic vesicles, the *Cripto* hypomorph displays a single prosencephalic vesicle (arrow); the hindbrain appears unaffected. (L-N) Transverse sections through wild-type and *Cripto*$^{3loxP/null}$ mutant embryos at the late neural plate/early head-fold stages, stained with Nuclear Fast Red. The wild-type embryo (L) has a midline prechordal plate that is absent in the *Cripto* hypomorph (M,N, arrow). Scale bars: 500 μm in A,D,E,H,I; 200 μm in B,C,F,G,J,K; 50 μm in L-N. di, diencephalic vesicles; hb, hindbrain; nt, neural tube; op, optic vesicles; pp, prechordal plate; so, somite pairs; te, telencephalic vesicles.

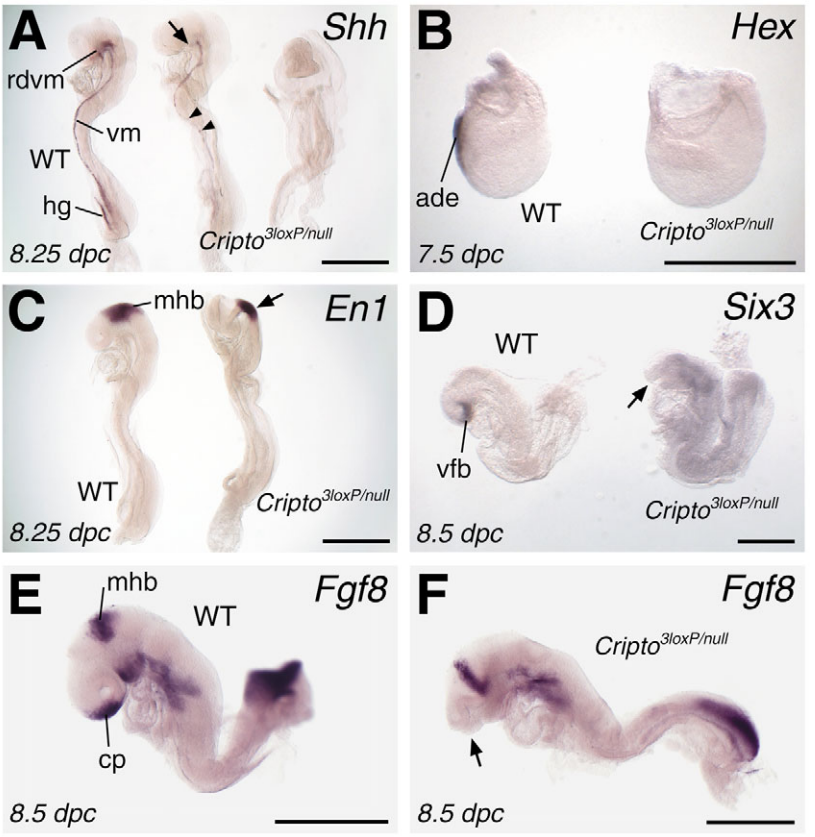

Fig. 3. Marker analysis of *Cripto*$^{3loxP/null}$ embryos. (A) Expression of *Shh* in wild-type and two *Cripto*$^{3loxP/null}$ littermates at 8.25 dpc. Expression in the rostral diencephalic ventral midline, ventral midline and hindgut is completely (arrow) or partially (arrowheads) absent in the less severely affected *Cripto*$^{3loxP/null}$ embryo (middle) and is abolished in the more severely affected embryo (right). (B) Expression of *Hex* in the anterior definitive endoderm at 7.5 dpc is lost in a *Cripto*$^{3loxP/null}$ littermate. (C) *En1* expression around the midbrain-hindbrain boundary in both wild-type and *Cripto* hypomorph embryos. (D) *Six3* marks the ventral forebrain but is absent in a *Cripto*$^{3loxP/null}$ littermate. (E,F) *Fgf8* is expressed in the telencephalic commissural plate and the midbrain/hindbrain boundary (E), but is absent from the anterior end of a *Cripto*$^{3loxP/null}$ embryo (F). Scale bars: 500 μm. cp, commissural plate; hg, hindgut; mhb, midbrain-hindbrain boundary; rdvm, rostral diencephalic ventral midline; vfb, ventral forebrain; vm, ventral midline.

+/+ chimeras displayed abnormal phenotypes, which resembled those of hypomorphic *Cripto*$^{3loxP/null}$ mutants (Fig. 6K,L); interestingly, there was abundant mesodermal contribution of marked cells even in the most severely affected chimeras (Fig. 6L).

In a second approach for chimera analysis, we used marked *Cripto*$^{lacZ/del}$ ES cells, which were derived from crosses of *Rosa26/+; Cripto*$^{del/+}$ mice with *Cripto*$^{lacZ/+}$ heterozygotes (Materials and methods) for microinjection into unmarked wild-type host blastocysts. In analysis of seven sectioned embryos (40-70% chimerism) at head-fold stages, we found an identical unbiased contribution of *Cripto* null mutant cells to derivatives of all three germ layers, including the prechordal plate, midline neuroectoderm and foregut endoderm (Fig. 6M-O). Thus, both methods of chimera analysis demonstrate that *Cripto* acts non-cell-autonomously in the axial mesendoderm and anterior definitive endoderm.

Addition of soluble Cripto to chick tissues suppresses posterior mesodermal fates and promotes anterior mesendodermal fates

The non-autonomous function of *Cripto* suggests that Cripto might act as a secreted trans-acting factor in the differentiation of anterior mesendoderm cell types, a process known to be dosage-sensitive for Nodal pathway activity (Agius et al., 2000; Dunn et al., 2004; Gritsman et al., 2000; Vincent et al., 2003). Consistent with this possibility, chick *Cripto* (also known as *CFC*) is expressed in the anterior primitive streak/Hensen's node at HH stages 3 and 4, as well as in notochord and prechordal plate at stages 5 and 6 (Colas and Schoenwolf, 2000; Schlange et al., 2001). To determine whether soluble Cripto protein might affect the differentiation of anterior mesendodermal cell types, we used chick embryos to assay the activity of Cripto-containing conditioned medium (Minchiotti et al., 2000; Yan et al., 2002).

Initially, we examined cell differentiation in node or head process mesoderm explants cultured in control medium, or medium conditioned by untransfected 293T cells. When HH stage 4^{-}-4 Hensen's node explants were cultured under these conditions (Fig. 7A), *Gsc*-expressing prechordal mesoderm cells, *Hex*-expressing anterior endoderm cells and 3B9-expressing notochord cells differentiated from the explanted node (n=20; Fig. 7B-D, data not shown). By contrast, when posterior head process mesoderm from HH stage 5 embryos was cultured (Fig. 7E), neither *Gsc*-expressing prechordal mesoderm cells nor *Hex*-expressing anterior endoderm cells was detected; however, differentiating notochord cells marked by the cell surface marker 3B9 were detected (n=30) (Fig. 7F-H, data not shown).

By contrast, addition of Cripto-conditioned medium evoked a very distinct pattern of differentiated cell types within node and head process mesoderm explants. When Cripto-conditioned medium was added to HH stage 4^{-}-4 Hensen's node explants, the differentiation of 3B9-expressing notochord cells was prevented (80%, n=20) (Fig. 7L), but robust differentiation of *Gsc*- and *Hex*-expressing cells was observed (100%, n=16) (Fig. 7J,K). This suggests that soluble Cripto protein can promote the differentiation of more anterior

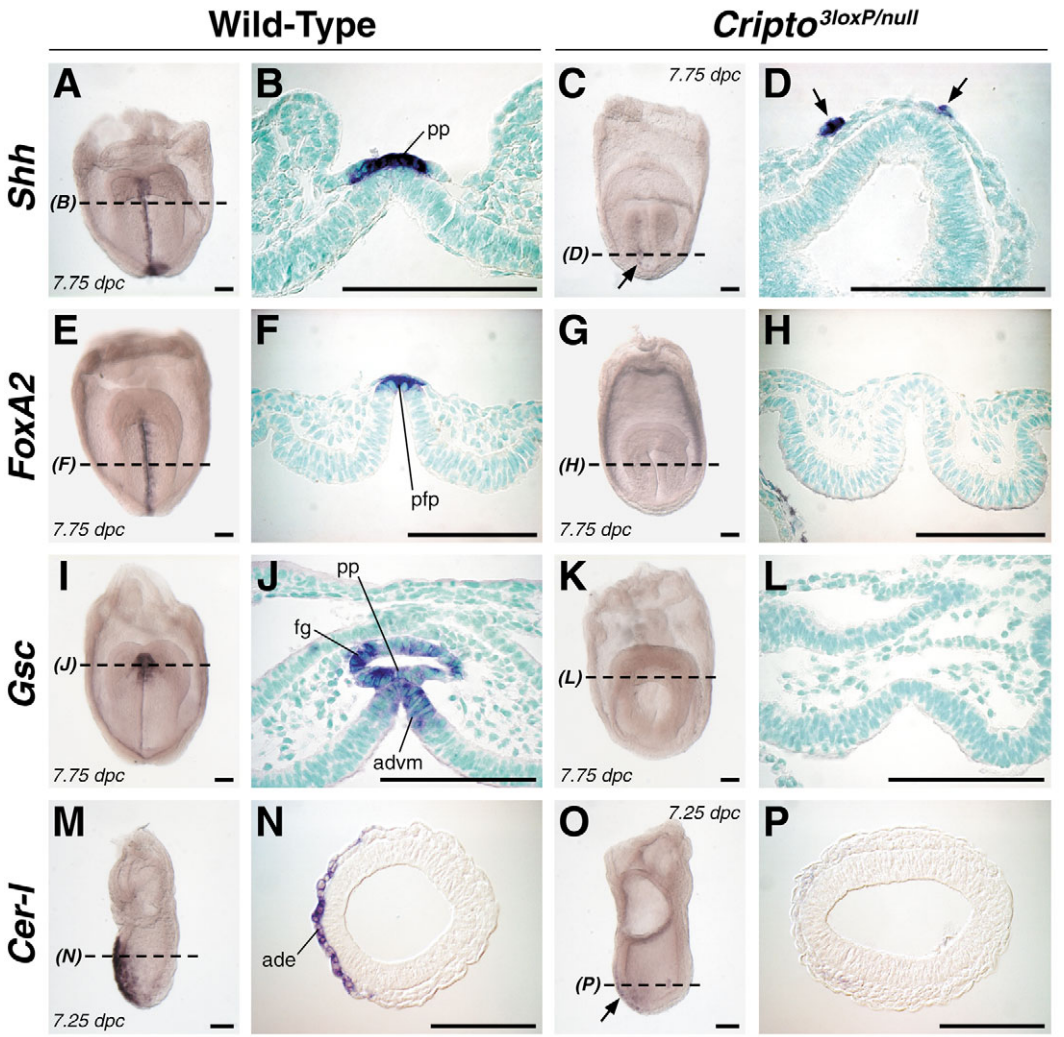

Fig. 4. Axial mesendoderm/definitive endoderm defects in *Cripto*$^{3loxP/null}$ embryos. Wild-type and *Cripto*$^{3loxP/null}$ embryos at the late head-fold stage (A-L) or early neural plate stage (M-P) are shown as whole mounts and corresponding transverse sections; B,D,F,H,J,L are counterstained with Methyl Green. (A-D) Expression of *Shh* in the prechordal plate is absent in the *Cripto*$^{3loxP/null}$ embryo; instead, a small number of expressing cells (arrows) can be found displaced from the axial midline. (E-H) Expression of *Foxa2* in the notochordal plate and prospective floor plate is absent in the *Cripto*$^{3loxP/null}$ embryo. (I-L) *Gsc* expression in the prechordal plate, anterior diencephalic ventral midline neuroectoderm and foregut endoderm is completely abolished in the *Cripto*$^{3loxP/null}$ mutant. (M-P) Expression of *Cer1* marks the anterior definitive endoderm, but is mostly absent except for scattered staining cells (arrow) in the *Cripto* hypomorph. Scale bars: 100 μm. ade, anterior definitive endoderm; advm, anterior diencephalic ventral midline; fg, foregut endoderm; pfp, prospective floor plate; pp, prechordal plate.

mesendodermal cell types (prechordal mesoderm and anterior endoderm), at the expense of posterior notochord cells. In support of this interpretation, when HH stage 5 posterior head process mesoderm was exposed to Cripto, *Gsc*-expressing prechordal mesoderm cells were detected in the central component of the explant, while *Hex*-expressing anterior endodermal cells were detected in peripheral regions of the explant (80%, *n*=10) (Fig. 7N,O). Concomitantly, the differentiation of 3B9-expressing notochord cells was prevented (80%, *n*=10) (Fig. 7P).

To examine whether Cripto can rapidly elicit a change in cellular fate, we used a sensitive real-time quantitative RT-PCR assay to examine the loss of notochord and induction of prechordal mesoderm properties in HH stage 5 posterior head process mesoderm. Explants were cultured in the absence or presence of Cripto-conditioned medium, and simultaneously monitored for expression of the prechordal mesoderm marker *Gsc* and the early notochord marker *Fgf10*. After a 4-hour culture period, Cripto addition caused an increase in *Gsc* expression and a concomitant decrease in *Fgf10* expression (*n*=7) (Fig. 7I,M).

We next established whether Cripto could similarly elicit a change in fate of axial mesodermal cells in vivo, promoting a prechordal mesoderm fate at the expense of notochord cell fate. Beads soaked in medium containing Cripto protein, or control medium, were implanted adjacent to Hensen's node of HH stage 4^{-}-4 chick embryos (*n*=6 each; Fig. 7Q), and the embryos were allowed to develop in ovo to HH stage 8-9 (Fig. 7U). In control-operated embryos, axial mesoderm displayed the normal phenotypic properties of notochord cells, as no

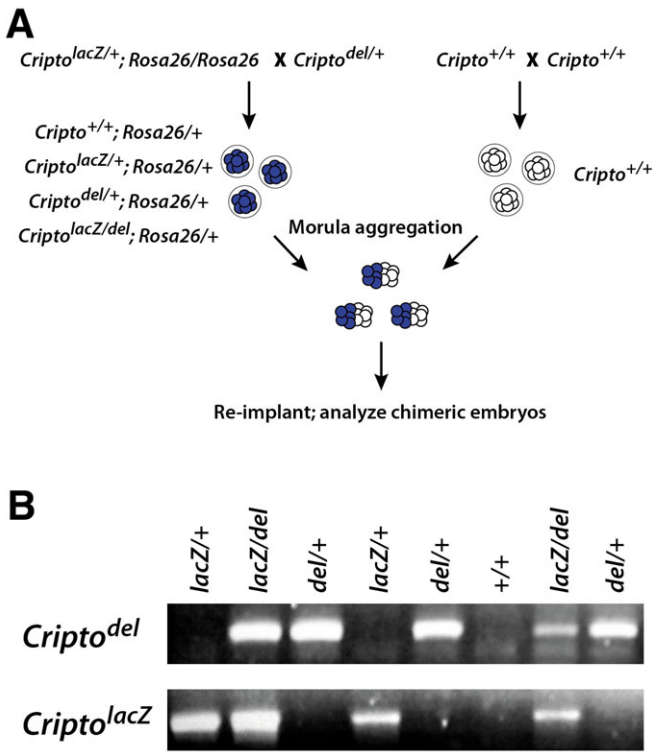

Fig. 5. Strategy for analysis of *Cripto* in aggregation chimeras. (A) Morula aggregation is performed between wild-type unmarked embryos and *Rosa26*-marked embryos from a cross between *Cripto* heterozygous parents [adapted from Rivera-Perez et al. (Rivera-Perez et al., 1999)]. One-quarter of the chimeras will contain marked *Cripto*-null cells (*Rosa26/+; Cripto*$^{lacZ/del}$↔ +/+), while the remaining three-quarters will be phenotypically wild type and serve as internal controls. (B) Extra-embryonic regions from β-galactosidase-stained chimeric embryos genotyped by PCR; analysis of a representative litter is shown.

expression of *Gsc* was detected (Fig. 7R), but the cells co-expressed Shh and 3B9 (Fig. 7S,T). By contrast, in embryos exposed to Cripto-conditioned medium, axial mesoderm at an equivalent rostrocaudal level (Fig. 7U) appeared to be anteriorized. Although situated adjacent to somites, axial mesoderm cells expressed the prechordal mesoderm marker, *Gsc* (Fig. 7V), as well as Shh (Fig. 7W), but expression of 3B9 was eliminated (Fig. 7X).

Finally, we examined whether the ability of exogenous Cripto to effect fate changes in axial mesoderm is dependent upon Nodal signaling. To do so, we utilized SB-43152, a small molecule inhibitor of the type I receptors ALK4/5/7 (Inman et al., 2002), to antagonize the Nodal receptors ALK4 and ALK7 (Reissmann et al., 2001; Yan et al., 2002; Yeo and Whitman, 2001). Culture of HH stage 5 posterior head process

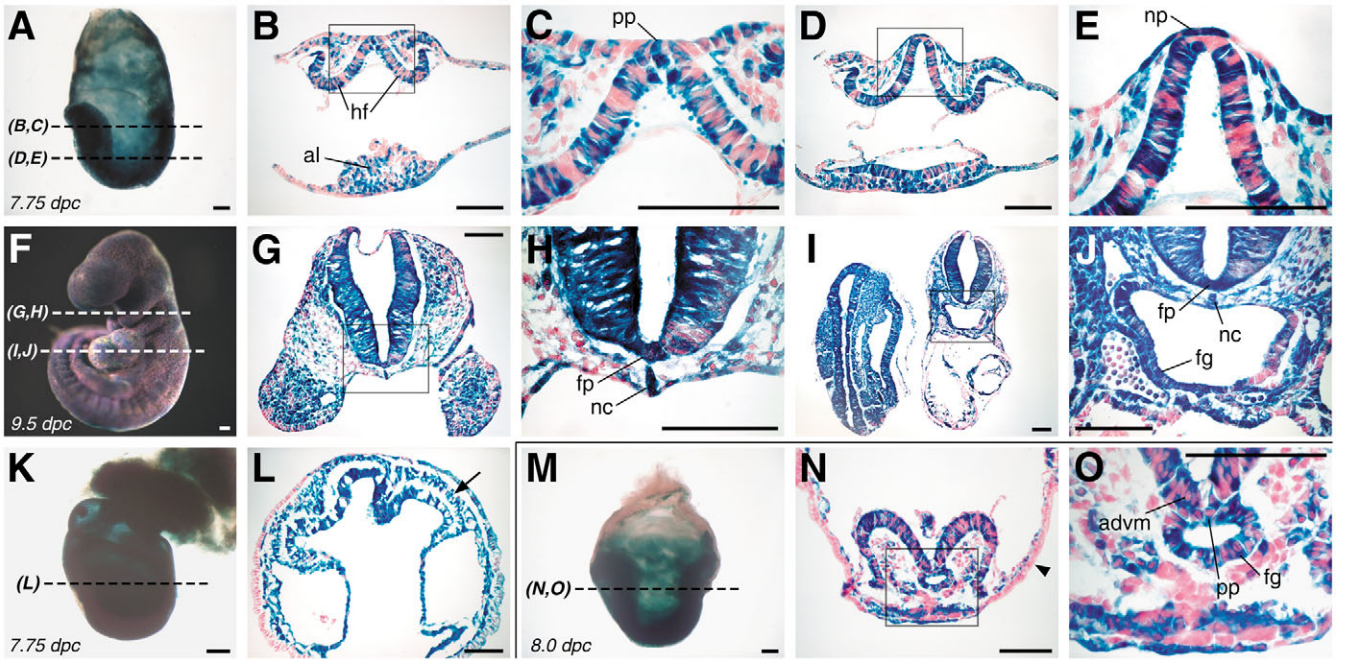

Fig. 6. Contribution of *Cripto* null mutant cells to prechordal mesoderm, notochord and foregut endoderm in chimeric embryos. (A-L) Analysis of *Rosa26/+; Cripto*$^{lacZ/del}$↔ +/+ chimeras generated by morula aggregation; whole-mount embryos were stained for β-galactosidase activity, and cryosections were counterstained with Nuclear Fast Red. (A-E) Medium-grade *Rosa26/+; Cripto*$^{lacZ/del}$↔ +/+ chimera at the late head-fold stage. Transverse sections (B,D) show random distribution of marked *Cripto* mutant cells in the headfolds and allantois; high-power views (C,E) show contribution of marked *Cripto* mutant cells to the prechordal plate and notochordal plate. (F-J) Medium-high-grade *Rosa26/+; Cripto*$^{lacZ/del}$↔ +/+ chimera at 9.5 dpc. Marked *Cripto* mutant cells contribute with high efficiency to all tissues examined (G,I); high-power views (H,J) show contribution of marked *Cripto* mutant cells to the notochord, floor plate and foregut endoderm. (K,L) High-grade *Rosa26/+; Cripto*$^{lacZ/del}$↔ +/+ chimera with abnormal morphology; note the presence of mesoderm (arrow in L). (M-O) Analysis of medium-grade chimera generated by blastocyst injection of marked *Cripto*$^{lacZ/del}$ ES cells. Mutant cells contribute efficiently to the prechordal plate, anterior diencephalic ventral midline and foregut endoderm. Scale bars: 100 μm. advm, anterior diencephalic ventral midline; al, allantois; fg, foregut endoderm; fp, floor plate; hf, headfolds; nc, notochord; np, notochordal plate; pp, prechordal plate.

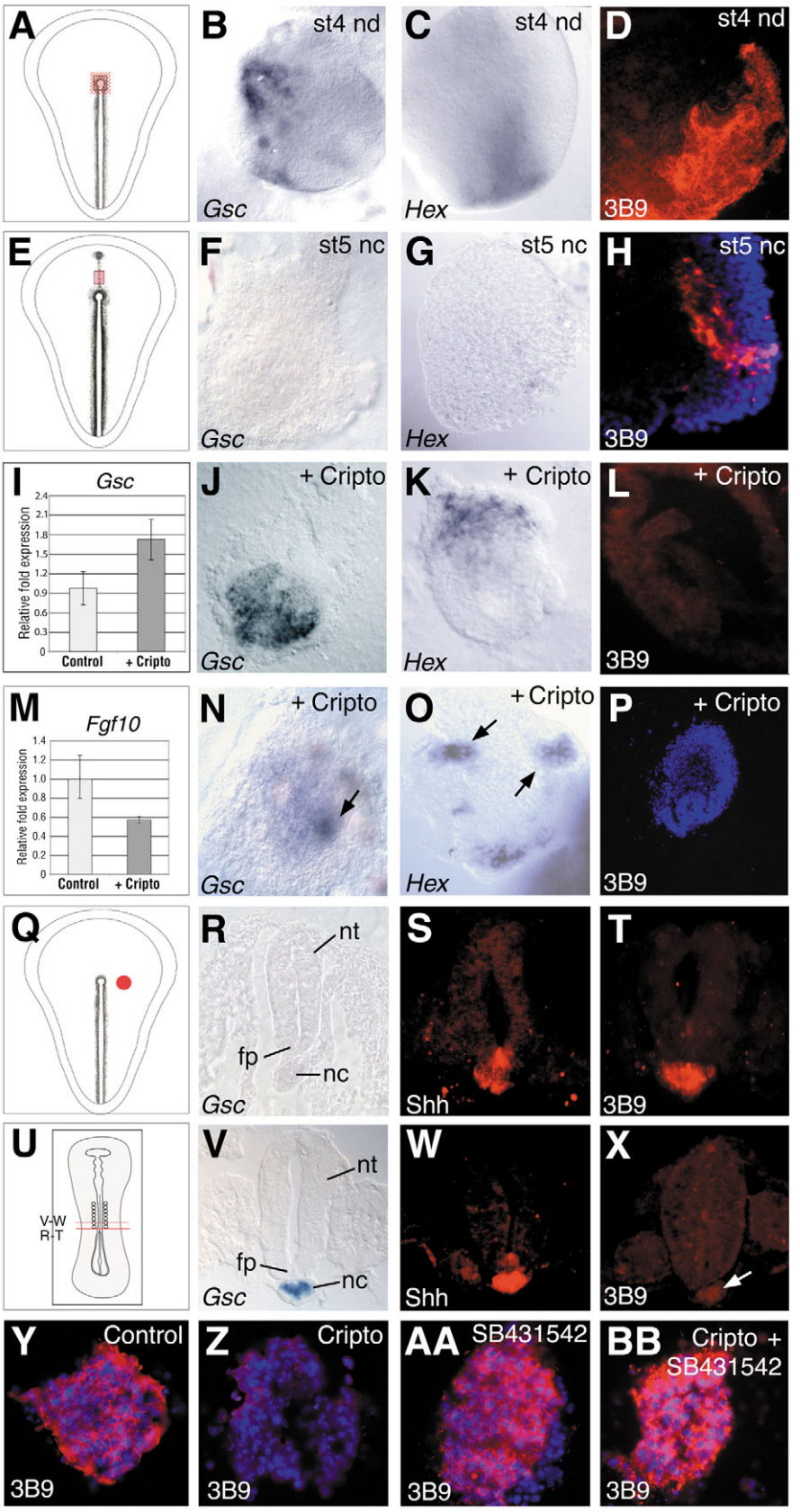

Fig. 7. Addition of exogenous Cripto alters the differentiation of chick node/head process mesoderm explants. (A,E) Schematic drawings showing regions dissected at HH stage 4⁻-4 (A) and HH stage 5 (E). (B-D,J-L) Explants of HH stage 4 Hensen's node cultured in vitro for 20 hours in the presence of 293T cell conditioned medium, either untransfected (B-D) or transfected with *Cripto* (J-L). *Gsc*-expressing prechordal mesoderm and *Hex*-expressing anterior endoderm differentiate with or without Cripto (B,C,J,K). 3B9-expressing notochord cells differentiate in control cultures (D) but not in explants exposed to Cripto (L). (F-I,M-P) Explants of HH stage 5 posterior head process mesoderm cultured in vitro for 20 hours (F-H,N-P) or 4 hours (I,M). Control cultures express 3B9 (H) and *Fgf10* (M) but not *Gsc* or *Hex* (F,G,M). Explants exposed to Cripto protein express *Gsc* and *Hex* (I,N,O), but downregulate 3B9 and *Fgf10* (M,P). Explant cultures (H,P) were counterstained with DAPI. (Q,U) Schematic drawings showing bead implant at HH stage 4 (Q) and level of sections analyzed at HH stage 9 (U). (R-T,V-X) Serial adjacent sections of HH stage 9 embryos, in which control beads (R-T) or Cripto-soaked beads (V-X) were placed adjacent to Hensen's node at HH stage 4. Axial mesoderm cells of control embryos display notochord properties, expressing 3B9 and Shh, but not *Gsc* (R-T). Axial mesoderm cells of Cripto-exposed embryos display prechordal mesoderm properties, expressing Shh and *Gsc*, but not 3B9 (V-X). (Y-BB) Explants of HH stage 5 head process mesoderm cultured in vitro for 20 hours. Control cultures and cultures exposed to SB-431542 express 3B9 (Y,AA). Cripto prevents expression of 3B9 (Z). The Cripto-mediated loss of 3B9 is abolished by treatment with SB-431542 (BB).

mesoderm with SB-43152 alone did not result in the loss of the notochord marker 3B9, appearing similar to control explants (n=9) (Fig. 7Y,AA). However, SB-43152 eliminated the ability of Cripto to anteriorize axial mesoderm, as culture of HH stage 5 head process mesoderm with Cripto resulted in loss of 3B9 and induction of *Gsc* and *Hex* (Fig. 7I,M-P,Z), while culture with Cripto and SB-43152 resulted in the sustained expression of 3B9 (80%, n=20) and no induction of *Gsc* or *Hex* (n=6 each) (Fig. 7BB, data not shown).

In summary, our findings in these gain-of-function assays show the ability of Cripto to act as a soluble trans-acting factor, eliciting effects consistent with increased Nodal signaling activity. These data strongly suggest that the non-autonomous requirement for *Cripto* in axial mesendoderm formation reflects the ability of Cripto protein to act intercellularly in vivo.

Discussion

Our analyses demonstrate that *Cripto* is transiently expressed in precursors of the axial mesendoderm and definitive endoderm, and is essential for formation and differentiation of these tissues. This requirement for *Cripto* is non-cell-autonomous, as null mutant cells readily contribute to the axial mesodendoderm in chimeric mouse embryos, and soluble Cripto protein elicits Nodal-dependent effects on axial mesoderm in chick embryos. In conjunction with analyses of other Nodal pathway components, our findings provide evidence that Cripto protein can act as an intercellular trans-acting factor in vivo.

Role of *Cripto* in axial midline formation

The requirement of *Cripto* in axial mesendoderm and definitive endoderm strongly indicates that Cripto is required for Nodal signaling in these tissues and/or their progenitors. Indeed, null and/or hypomorphic mouse mutants for several Nodal pathway components display similar phenotypes to those of *Cripto* hypomorphs, including mutants for Nodal (Lowe et al., 2001; Norris et al., 2002), the type II activin receptors ActRIIA and ActRIIB (Song et al., 1999), the intracellular signal transducers Smad2 and Smad3 (Dunn et al., 2004; Heyer et al., 1999; Vincent et al., 2003), Smad4 (Chu et al., 2004), and the winged-helix transcription factor FoxH1 (Hoodless et al., 2001; Pogoda et al., 2000; Sirotkin et al., 2000; Yamamoto et al., 2001). Nonetheless, we note that Cripto may also have Nodal-independent functions. For example, the EGF-CFC protein Oep has been proposed to act independently of Nodal in regulation of cell motility in the zebrafish blastoderm (Warga and Kane, 2003). In addition, cell culture studies have shown that Cripto can block Activin signaling in the absence of Nodal activity (Adkins et al., 2003; Gray et al., 2003). Finally, a recent study has found that the *Xenopus* EGF-CFC protein FRL-1 can mediate signaling by Wnt11 in the canonical Wnt/β-catenin pathway during dorsal axis formation (Tao et al., 2005).

Given the transient expression of *Cripto* during gastrulation, and the early appearance of axial midline defects in *Cripto* hypomorphs, the requirement for *Cripto* function (and hence Nodal signaling) is likely to occur in axial mesendoderm progenitors within or shortly after their emergence from the anterior primitive streak. This temporal requirement may also coincide with the timing of Nodal signaling from the axial mesoderm to the overlying neuroectoderm in floor plate induction (Patten et al., 2003) (reviewed by Placzek and Briscoe, 2005). Although our investigation of the *Cripto* hypomorph phenotype does not directly address whether *Cripto* function is also required in the floor plate, the chimera analysis suggests that such a role for *Cripto* would also be non-cell-autonomous (Fig. 6H,J; data not shown).

Our analyses of mutant mice show that reductions of *Cripto* activity affect rostral midline structures (prechordal plate) in preference to caudal structures (notochord), as indicated by the spectrum of holoprosencephaly phenotypes in Fig. 2, while exposure of chick cells to exogenous Cripto both in vitro and in vivo increases prechordal mesoderm at the expense of notochord. These results complement previous observations that levels of *Nodal* activity specify the rostrocaudal identity of axial mesoderm (Agius et al., 2000; Gritsman et al., 2000; Lowe et al., 2001; Norris and Robertson, 1999; Thisse et al., 2000; Vincent et al., 2003). More generally, our findings demonstrate that reduction of *Cripto* activity can lead to a 'pinhead' phenotype that resembles that of zygotic *oep* mutants (Schier et al., 1997). This observation, together with the identification of a *Cripto* loss-of-function mutation in a human patient with midline forebrain defects (de la Cruz et al., 2002), provides additional support for the evolutionary conservation of *EGF-CFC* functions.

Non-cell-autonomy of Cripto implies its intercellular activity

In principle, the experimental observation of non-cell-autonomy implies that the gene product, or one of its major regulatory targets, mediates a cell-cell signaling event. In some cases, genes encoding proteins with intracellular functions, such as transcription factors, can nonetheless display non-cell-autonomy (e.g. Rhinn et al., 1999). However, analysis of the Nodal pathway component FoxH1 has shown that this transcription factor is required cell-autonomously for axial mesendoderm and definitive endoderm formation (Hoodless et al., 2001). Thus, the upstream extracellular component Cripto acts non-cell-autonomously in the Nodal pathway, but the downstream transcription factor FoxH1 is cell-autonomous (Fig. 8A). Moreover, chimera analysis of *Smad2* has demonstrated its cell-autonomous requirement in definitive endoderm (Tremblay et al., 2000). Based on this pathway relationship (Fig. 8A), we conclude that it is Cripto itself, not one of its regulatory targets, that can act in trans as an intercellular mediator of Nodal signaling.

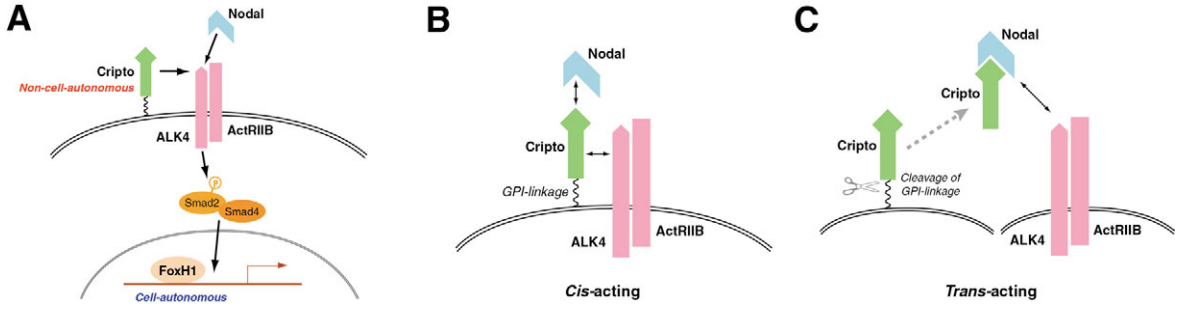

Fig. 8. (A) Cell-autonomy and non-cell-autonomy of genes in the Nodal signaling pathway [adapted from Schier and Shen (Schier and Shen, 2000)]. (B,C) Schematic model for Cripto function in mediating Nodal activity as a cis-acting GPI-linked co-receptor (B), as well as a trans-acting soluble factor (C) [adapted from Yan et al. (Yan et al., 2002)].

The intercellular activity of Cripto may reflect its ability to be released from the cell surface in an active form, as we have previously shown (Yan et al., 2002). As Cripto is a GPI-linked protein, several possible mechanisms may explain its release from the cell surface. These include protein shedding due to cleavage of the GPI anchor (e.g. Kondoh et al., 2005; Metz et al., 1994), or formation of membrane vesicles (argosomes) that can traverse neighboring cells (Greco et al., 2001). Moreover, there are several precedents for shedding of GPI-linked proteins under physiological circumstances, such as the regulated proteolytic cleavage of ephrin-A2 during neuronal axon repulsion (Hattori et al., 2000), or the release of the glypican Dally-like, which modulates Wingless signaling in *Drosophila* (Kreuger et al., 2004). However, we note that our findings show only that Cripto is capable of acting intercellularly under physiological circumstances in vivo, but do not necessarily imply that such an activity is utilized during wild-type development. For example, GFRα is a GPI-linked co-receptor that has been proposed to act in trans to provide a response to GDNF family ligands in cells that express the Ret receptor but not GFRα (e.g. Mikaels-Edman et al., 2003; Paratcha et al., 2001), but this model has been challenged by a recent study showing the absence of Ret-independent GFRα function in vivo (Enomoto et al., 2004).

Our data may provide a unifying basis for two bodies of literature on Cripto activity and function that have previously seemed difficult to reconcile. While work in zebrafish, frog and mouse systems has supported a role for EGF-CFC proteins as cis-acting co-receptors for Nodal ligands, there is also ample evidence for trans-acting soluble activities of Cripto, particularly in cell culture. Notably, work from the Salomon laboratory has shown that recombinant Cripto protein or peptide fragments can elicit specific responses in cell culture, for example resulting in activation of the MAPK pathway (Bianco et al., 2002; Bianco et al., 1999; Bianco et al., 2003; De Santis et al., 1997; Ebert et al., 1999; Kannan et al., 1997). In some cases, these cellular responses are due to activation of the Nodal pathway, whereas other Cripto activities appear to be Nodal-independent (Bianco et al., 2002; Bianco et al., 2003). Other investigators have found that truncated Cripto protein lacking the C-terminal GPI anchor can rescue the cardiac differentiation defects of *Cripto*-deficient ES cells (Parisi et al., 2003), and that injection of truncated Oep protein into the syncytial yolk layer of zebrafish embryos will rescue the *oep* mutant phenotype (Minchiotti et al., 2001). Finally, our studies using a reconstituted Nodal signaling assay in mammalian cells have shown that the ability of soluble Cripto to signal in this system is Nodal- and FoxH1-dependent (Yan et al., 2002). All of these data support a model in which Cripto possesses intrinsic activity as a non-membrane-associated protein that can mediate Nodal signaling in trans (Fig. 8B,C).

Consistent with possible trans-acting functions, several studies have reported phenotypes associated with overexpression/ectopic expression of *EGF-CFC* genes in vivo. For example, overexpression of wild-type human *Cryptic* – but not mouse *Cryptic* – in zebrafish leads to developmental delays and abnormal gastrulation movements (Bamford et al., 2000), while overexpression of secreted forms of *oep* can promote dorsoanterior development (Kiecker et al., 2000). In chick embryos, implantation of cells expressing human *Cryptic*, mouse *Cryptic* or chick *Cripto* on the right side of Hensen's node leads to randomization of cardiac looping (Schlange et al., 2001). Finally, overexpression of frog *FRL-1* in *Xenopus* animal caps results in neural induction in the absence of mesoderm formation (Kinoshita et al., 1995; Yabe et al., 2003; Yokota et al., 2003).

By contrast, other studies have shown the absence of a gain-of-function phenotype following overexpression of wild-type *oep* in fish (Bamford et al., 2000; Gritsman et al., 1999; Zhang et al., 1998). Moreover, rigorous cell transplantation assays have established the strict cell-autonomy of *oep* function in several tissues (Gritsman et al., 2000; Schier et al., 1997; Strahle et al., 1997; Warga and Kane, 2003). These opposite findings in zebrafish versus mice (and chick) strongly suggest an underlying divergence in the mechanism of EGF-CFC function. Therefore, despite the evolutionary conservation of *EGF-CFC* function in axial midline formation, EGF-CFC proteins may utilize disparate non-conserved molecular mechanisms for this essential developmental process.

We thank Tony Wynshaw-Boris and Heiner Westphal for the *EIIa-Cre* mice and advice on the partial deletion strategy, Jose Belo, Alex Joyner, Gail Martin, Andy McMahon, Guillermo Oliver, Janet Rossant and the late Rosa Beddington for generously providing probes, and Cory Abate-Shen, Rebecca Burdine, Ken Irvine and Ruth Steward for helpful discussions and comments on the manuscript. This work was supported by grants from the American Heart Association (J.D.), the Leukemia and Lymphoma Society (J.D.), the Medical Research Council of Great Britain (M.P.), the Wellcome Trust (M.P.) and the NIH (M.M.S.).

References

Adkins, H. B., Bianco, C., Schiffer, S. G., Rayhorn, P., Zafari, M., Cheung, A. E., Orozco, O., Olson, D., De Luca, A., Chen, L. L. et al. (2003). Antibody blockade of the Cripto CFC domain suppresses tumor cell growth in vivo. *J. Clin. Invest.* **112**, 575-587.

Agius, E., Oelgeschlager, M., Wessely, O., Kemp, C. and De Robertis, E. M. (2000). Endodermal Nodal-related signals and mesoderm induction in Xenopus. *Development* **127**, 1173-1183.

Ang, S. L. and Rossant, J. (1994). HNF-3 beta is essential for node and notochord formation in mouse development. *Cell* **78**, 561-574.

Bamford, R. N., Roessler, E., Burdine, R. D., Saplakoglu, U., dela Cruz, J., Splitt, M., Towbin, J., Bowers, P., Marino, B., Schier, A. F. et al. (2000). Loss-of-function mutations in the EGF-CFC gene *CFC1* are associated with human left-right laterality defects. *Nat. Genet.* **26**, 365-369.

Belo, J. A., Bouwmeester, T., Leyns, L., Kertesz, N., Gallo, M., Follettie, M. and De Robertis, E. M. (1997). Cerberus-like is a secreted factor with neutralizing activity expressed in the anterior primitive endoderm of the mouse gastrula. *Mech. Dev.* **68**, 45-57.

Bianco, C., Kannan, S., De Santis, M., Seno, M., Tang, C. K., Martinez-Lacaci, I., Kim, N., Wallace-Jones, B., Lippman, M. E., Ebert, A. D. et al. (1999). Cripto-1 indirectly stimulates the tyrosine phosphorylation of erbB-4 through a novel receptor. *J. Biol. Chem.* **274**, 8624-8629.

Bianco, C., Adkins, H. B., Wechselberger, C., Seno, M., Normanno, N., De Luca, A., Sun, Y., Khan, N., Kenney, N., Ebert, A. et al. (2002). Cripto-1 activates nodal- and ALK4-dependent and -independent signaling pathways in mammary epithelial cells. *Mol. Cell. Biol.* **22**, 2586-2597.

Bianco, C., Strizzi, L., Rehman, A., Normanno, N., Wechselberger, C., Sun, Y., Khan, N., Hirota, M., Adkins, H., Williams, K. et al. (2003). A Nodal- and ALK4-independent signaling pathway activated by Cripto-1 through Glypican-1 and c-Src. *Cancer Res.* **63**, 1192-1197.

Chu, G. C., Dunn, N. R., Anderson, D. C., Oxburgh, L. and Robertson, E. J. (2004). Differential requirements for Smad4 in TGFbeta-dependent patterning of the early mouse embryo. *Development* **131**, 3501-3512.

Colas, J. F. and Schoenwolf, G. C. (2000). Subtractive hybridization identifies chick-cripto, a novel EGF-CFC ortholog expressed during gastrulation, neurulation and early cardiogenesis. *Gene* **255**, 205-217.

Crompton, M. R., Bartlett, T. J., MacGregor, A. D., Manfioletti, G., Buratti, E., Giancotti, V. and Goodwin, G. H. (1992). Identification of a

novel vertebrate homeobox gene expressed in haematopoietic cells. *Nucleic Acids Res*. **20**, 5661-5667.

Crossley, P. H. and Martin, G. R. (1995). The mouse Fgf8 gene encodes a family of polypeptides and is expressed in regions that direct outgrowth and patterning in the developing embryo. *Development* **121**, 439-451.

Davis, C. A. and Joyner, A. L. (1988). Expression patterns of the homeo box-containing genes En-1 and En-2 and the proto-oncogene int-1 diverge during mouse development. *Genes Dev*. **2**, 1736-1744.

de la Cruz, J. M., Bamford, R. N., Burdine, R. D., Roessler, E., Barkovich, A. J., Donnai, D., Schier, A. F. and Muenke, M. (2002). A loss-of-function mutation in the CFC domain of TDGF1 is associated with human forebrain defects. *Hum. Genet*. **110**, 422-428.

De Santis, M. L., Kannan, S., Smith, G. H., Seno, M., Bianco, C., Kim, N., Martinez-Lacaci, I., Wallace-Jones, B. and Salomon, D. S. (1997). Cripto-1 inhibits beta-casein expression in mammary epithelial cells through a p21ras-and phosphatidylinositol 3′-kinase-dependent pathway. *Cell Growth Differ*. **8**, 1257-1266.

Ding, J., Yang, L., Yan, Y. T., Chen, A., Desai, N., Wynshaw-Boris, A. and Shen, M. M. (1998). *Cripto* is required for correct orientation of the anterior-posterior axis in the mouse embryo. *Nature* **395**, 702-707.

Dunn, N. R., Vincent, S. D., Oxburgh, L., Robertson, E. J. and Bikoff, E. K. (2004). Combinatorial activities of Smad2 and Smad3 regulate mesoderm formation and patterning in the mouse embryo. *Development* **131**, 1717-1728.

Ebert, A. D., Wechselberger, C., Frank, S., Wallace-Jones, B., Seno, M., Martinez-Lacaci, I., Bianco, C., De Santis, M., Weitzel, H. K. and Salomon, D. S. (1999). Cripto-1 induces phosphatidylinositol 3′-kinase-dependent phsophorylation of AKT and glycogen synthase kinase 3β in human cervical carcinoma cells. *Cancer Res*. **59**, 4502-4505.

Echelard, Y., Epstein, D. J., St-Jacques, B., Shen, L., Mohler, J., McMahon, J. A. and McMahon, A. P. (1993). Sonic hedgehog, a member of a family of putative signaling molecules, is implicated in the regulation of CNS polarity. *Cell* **75**, 1417-1430.

Enomoto, H., Hughes, I., Golden, J., Baloh, R. H., Yonemura, S., Heuckeroth, R. O., Johnson, E. M., Jr and Milbrandt, J. (2004). GFRalpha1 expression in cells lacking RET is dispensable for organogenesis and nerve regeneration. *Neuron* **44**, 623-636.

Ericson, J., Morton, S., Kawakami, A., Roelink, H. and Jessell, T. M. (1996). Two critical periods of Sonic Hedgehog signaling required for the specification of motor neuron identity. *Cell* **87**, 661-673.

Friedrich, G. and Soriano, P. (1991). Promoter traps in embryonic stem cells: a genetic screen to identify and mutate developmental genes in mice. *Genes Dev*. **5**, 1513-1523.

Gray, P. C., Harrison, C. A. and Vale, W. (2003). Cripto forms a complex with activin and type II activin receptors and can block activin signaling. *Proc. Natl. Acad. Sci. USA* **100**, 5193-5198.

Greco, V., Hannus, M. and Eaton, S. (2001). Argosomes: a potential vehicle for the spread of morphogens through epithelia. *Cell* **106**, 633-645.

Gritsman, K., Zhang, J., Cheng, S., Heckscher, E., Talbot, W. S. and Schier, A. F. (1999). The EGF-CFC protein one-eyed pinhead is essential for nodal signaling. *Cell* **97**, 121-132.

Gritsman, K., Talbot, W. S. and Schier, A. F. (2000). Nodal signaling patterns the organizer. *Development* **127**, 921-932.

Hattori, M., Osterfield, M. and Flanagan, J. G. (2000). Regulated cleavage of a contact-mediated axon repellent. *Science* **289**, 1360-1365.

Heyer, J., Escalante-Alcalde, D., Lia, M., Boettinger, E., Edelmann, W., Stewart, C. L. and Kucherlapati, R. (1999). Postgastrulation Smad2-deficient embryos show defects in embryo turning and anterior morphogenesis. *Proc. Natl. Acad. Sci. USA* **96**, 12595-12600.

Hoodless, P. A., Pye, M., Chazaud, C., Labbe, E., Attisano, L., Rossant, J. and Wrana, J. L. (2001). FoxH1 (Fast) functions to specify the anterior primitive streak in the mouse. *Genes Dev*. **15**, 1257-1271.

Hume, C. R. and Dodd, J. (1993). Cwnt-8C: a novel Wnt gene with a potential role in primitive streak formation and hindbrain organization. *Development* **119**, 1147-1160.

Inman, G. J., Nicolas, F. J., Callahan, J. F., Harling, J. D., Gaster, L. M., Reith, A. D., Laping, N. J. and Hill, C. S. (2002). SB-431542 is a potent and specific inhibitor of transforming growth factor-beta superfamily type I activin receptor-like kinase (ALK) receptors ALK4, ALK5, and ALK7. *Mol. Pharmacol*. **62**, 65-74.

Kannan, S., De Santis, M., Lohmeyer, M., Riese, D. J., 2nd, Smith, G. H., Hynes, N., Seno, M., Brandt, R., Bianco, C., Persico, G. et al. (1997). Cripto enhances the tyrosine phosphorylation of Shc and activates mitogen-activated protein kinase (MAPK) in mammary epithelial cells. *J. Biol. Chem*. **272**, 3330-3335.

Kiecker, C. and Niehrs, C. (2001). The role of prechordal mesendoderm in neural patterning. *Curr. Opin. Neurobiol*. **11**, 27-33.

Kiecker, C., Muller, F., Wu, W., Glinka, A., Strahle, U. and Niehrs, C. (2000). Phenotypic effects in Xenopus and zebrafish suggest that one-eyed pinhead functions as antagonist of BMP signalling. *Mech. Dev*. **94**, 37-46.

Kinder, S. J., Tsang, T. E., Wakamiya, M., Sasaki, H., Behringer, R. R., Nagy, A. and Tam, P. P. (2001). The organizer of the mouse gastrula is composed of a dynamic population of progenitor cells for the axial mesoderm. *Development* **128**, 3623-3634.

Kinoshita, N., Minshull, J. and Kirschner, M. W. (1995). The identification of two novel ligands of the FGF receptor by a yeast screening method and their activity in Xenopus development. *Cell* **83**, 621-630.

Kondoh, G., Tojo, H., Nakatani, Y., Komazawa, N., Murata, C., Yamagata, K., Maeda, Y., Kinoshita, T., Okabe, M., Taguchi, R. et al. (2005). Angiotensin-converting enzyme is a GPI-anchored protein releasing factor crucial for fertilization. *Nat. Med*. **11**, 160-166.

Kreuger, J., Perez, L., Giraldez, A. J. and Cohen, S. M. (2004). Opposing activities of Dally-like glypican at high and low levels of Wingless morphogen activity. *Dev. Cell* **7**, 503-512.

Kumar, A., Novoselov, V., Celeste, A. J., Wolfman, N. M., ten Dijke, P. and Kuehn, M. R. (2001). Nodal signaling uses activin and transforming growth factor-beta receptor-regulated Smads. *J. Biol. Chem*. **276**, 656-661.

Lowe, L. A., Yamada, S. and Kuehn, M. R. (2001). Genetic dissection of nodal function in patterning the mouse embryo. *Development* **128**, 1831-1843.

Metz, C. N., Brunner, G., Choi-Muira, N. H., Nguyen, H., Gabrilove, J., Caras, I. W., Altszuler, N., Rifkin, D. B., Wilson, E. L. and Davitz, M. A. (1994). Release of GPI-anchored membrane proteins by a cell-associated GPI-specific phospholipase D. *EMBO J*. **13**, 1741-1751.

Meyers, E. N., Lewandoski, M. and Martin, G. R. (1998). An Fgf8 mutant allelic series generated by Cre- and Flp-mediated recombination. *Nat. Genet*. **18**, 136-141.

Mikaels-Edman, A., Baudet, C. and Ernfors, P. (2003). Soluble and bound forms of GFRalpha1 elicit different GDNF-independent neurite growth responses in primary sensory neurons. *Dev. Dyn*. **227**, 27-34.

Minchiotti, G., Parisi, S., Liguori, G., Signore, M., Lania, G., Adamson, E. D., Lago, C. T. and Persico, M. G. (2000). Membrane-anchorage of Cripto protein by glycosylphosphatidylinositol and its distribution during early mouse development. *Mech. Dev*. **90**, 133-142.

Minchiotti, G., Manco, G., Parisi, S., Lago, C. T., Rosa, F. and Persico, M. G. (2001). Structure-function analysis of the EGF-CFC family member Cripto identifies residues essential for nodal signalling. *Development* **128**, 4501-4510.

Nagy, A., Gertsenstein, M., Vintersten, K. and Behringer, R. (2003). *Manipulating the Mouse Embryo: A Laboratory Manual*. New York: Cold Spring Harbor Laboratory Press.

Norris, D. P. and Robertson, E. J. (1999). Asymmetric and node-specific nodal expression patterns are controlled by two distinct cis-acting regulatory elements. *Genes Dev*. **13**, 1575-1588.

Norris, D. P., Brennan, J., Bikoff, E. K. and Robertson, E. J. (2002). The FoxH1-dependent autoregulatory enhancer controls the level of Nodal signals in the mouse embryo. *Development* **129**, 3455-3468.

Ober, E. A., Field, H. A. and Stainier, D. Y. (2003). From endoderm formation to liver and pancreas development in zebrafish. *Mech. Dev*. **120**, 5-18.

Oliver, G., Mailhos, A., Wehr, R., Copeland, N. G., Jenkins, N. A. and Gruss, P. (1995). Six3, a murine homologue of the sine oculis gene, demarcates the most anterior border of the developing neural plate and is expressed during eye development. *Development* **121**, 4045-4055.

Paratcha, G., Ledda, F., Baars, L., Coulpier, M., Besset, V., Anders, J., Scott, R. and Ibanez, C. F. (2001). Released GFRalpha1 potentiates downstream signaling, neuronal survival, and differentiation via a novel mechanism of recruitment of c-Ret to lipid rafts. *Neuron* **29**, 171-184.

Parisi, S., D'Andrea, D., Lago, C. T., Adamson, E. D., Persico, M. G. and Minchiotti, G. (2003). Nodal-dependent Cripto signaling promotes cardiomyogenesis and redirects the neural fate of embryonic stem cells. *J. Cell Biol*. **163**, 303-314.

Patten, I., Kulesa, P., Shen, M. M., Fraser, S. and Placzek, M. (2003). Distinct modes of floor plate induction in the chick embryo. *Development* **130**, 4809-4821.

Placzek, M. and Briscoe, J. (2005). The floor plate: multiple cells, multiple signals. *Nat. Rev. Neurosci*. **6**, 230-240.

Placzek, M., Tessier-Lavigne, M., Jessell, T. and Dodd, J. (1990).

Orientation of commissural axons in vitro in response to a floor plate-derived chemoattractant. *Development* **110**, 19-30.

Placzek, M., Jessell, T. M. and Dodd, J. (1993). Induction of floor plate differentiation by contact-dependent, homeogenetic signals. *Development* **117**, 205-218.

Pogoda, H. M., Solnica-Krezel, L., Driever, W. and Meyer, D. (2000). The zebrafish forkhead transcription factor FoxH1/Fast1 is a modulator of nodal signaling required for organizer formation. *Curr. Biol.* **10**, 1041-1049.

Reissmann, E., Jornvall, H., Blokzijl, A., Andersson, O., Chang, C., Minchiotti, G., Persico, M. G., Ibanez, C. F. and Brivanlou, A. H. (2001). The orphan receptor ALK7 and the Activin receptor ALK4 mediate signaling by Nodal proteins during vertebrate development. *Genes Dev.* **15**, 2010-2022.

Rhinn, M., Dierich, A., Le Meur, M. and Ang, S. (1999). Cell autonomous and non-cell autonomous functions of Otx2 in patterning the rostral brain. *Development* **126**, 4295-4304.

Rivera-Perez, J. A., Wakamiya, M. and Behringer, R. R. (1999). Goosecoid acts cell autonomously in mesenchyme-derived tissues during craniofacial development. *Development* **126**, 3811-3821.

Schier, A. F. and Shen, M. M. (2000). Nodal signalling in vertebrate development. *Nature* **403**, 385-389.

Schier, A. F., Neuhauss, S. C. F., Helde, K. A., Talbot, W. S. and Driever, W. (1997). The *one-eyed pinhead* gene functions in mesoderm and endoderm formation in zebrafish and interacts with *no tail*. *Development* **124**, 327-342.

Schlange, T., Schnipkoweit, I., Andree, B., Ebert, A., Zile, M. H., Arnold, H. H. and Brand, T. (2001). Chick *cfc* controls *lefty1* expression in the embryonic midline and nodal expression in the lateral plate. *Dev. Biol.* **234**, 376-389.

Shalaby, F., Rossant, J., Yamaguchi, T. P., Gertsenstein, M., Wu, X.-F., Breitman, M. L. and Schuh, A. C. (1995). Failure of blood-island formation and vasculogenesis in Flk-1 deficient mice. *Nature* **376**, 62-66.

Shen, M. M. and Schier, A. F. (2000). The *EGF-CFC* gene family in vertebrate development. *Trends Genet.* **16**, 303-309.

Sirotkin, H. I., Gates, M. A., Kelly, P. D., Schier, A. F. and Talbot, W. S. (2000). *Fast1* is required for the development of dorsal axial structures in zebrafish. *Curr. Biol.* **10**, 1051-1054.

Song, J., Oh, S. P., Schrewe, H., Nomura, M., Lei, H., Okano, M., Gridley, T. and Li, E. (1999). The type II activin receptors are essential for egg cylinder growth, gastrulation, and rostral head development in mice. *Dev. Biol.* **213**, 157-169.

Strahle, U., Jesuthasan, S., Blader, P., Garcia-Villalba, P., Hatta, K. and Ingham, P. W. (1997). one-eyed pinhead is required for development of the ventral midline of the zebrafish (Danio rerio) neural tube. *Genes Funct.* **1**, 131-148.

Tam, P. P. and Beddington, R. S. (1987). The formation of mesodermal tissues in the mouse embryo during gastrulation and early organogenesis. *Development* **99**, 109-126.

Tam, P. P., Kanai-Azuma, M. and Kanai, Y. (2003). Early endoderm development in vertebrates: lineage differentiation and morphogenetic function. *Curr. Opin. Genet. Dev.* **13**, 393-400.

Tao, Q., Yokota, C., Puck, H., Kofron, M., Birsoy, B., Yan, D., Asashima, M., Wylie, C. C., Lin, X. and Heasman, J. (2005). Maternal Wnt11 activates the canonical Wnt signaling pathway required for axis formation in Xenopus embryos. *Cell* **120**, 857-871.

Thisse, B., Wright, C. V. and Thisse, C. (2000). Activin- and Nodal-related factors control antero-posterior patterning of the zebrafish embryo. *Nature* **403**, 425-428.

Thomas, P. Q., Brown, A. and Beddington, R. S. P. (1998). *Hex*: a homeobox gene revealing peri-implantation asymmetry in the mouse embryo and an early transient marker of endothelial cell precursors. *Development* **125**, 85-94.

Tremblay, K. D., Hoodless, P. A., Bikoff, E. K. and Robertson, E. J. (2000). Formation of the definitive endoderm in mouse is a Smad2-dependent process. *Development* **127**, 3079-3090.

Vincent, S. D., Dunn, N. R., Hayashi, S., Norris, D. P. and Robertson, E. J. (2003). Cell fate decisions within the mouse organizer are governed by graded Nodal signals. *Genes Dev.* **17**, 1646-1662.

Warga, R. M. and Kane, D. A. (2003). One-eyed pinhead regulates cell motility independent of Squint/Cyclops signaling. *Dev. Biol.* **261**, 391-411.

Wilson, S. W. and Houart, C. (2004). Early steps in the development of the forebrain. *Dev. Cell* **6**, 167-181.

Xu, C., Liguori, G., Persico, M. G. and Adamson, E. D. (1999). Abrogation of the Cripto gene in mouse leads to failure of postgastrulation morphogenesis and lack of differentiation of cardiomyocytes. *Development* **126**, 483-494.

Xu, X., Li, C., Garrett-Beal, L., Larson, D., Wynshaw-Boris, A. and Deng, C. X. (2001). Direct removal in the mouse of a floxed neo gene from a three-loxP conditional knockout allele by two novel approaches. *Genesis* **30**, 1-6.

Yabe, S. I., Tanegashima, K., Haramoto, Y., Takahashi, S., Fujii, T., Kozuma, S., Taketani, Y. and Asashima, M. (2003). FRL-1, a member of the EGF-CFC family, is essential for neural differentiation in Xenopus early development. *Development* **130**, 2071-2081.

Yamamoto, M., Meno, C., Sakai, Y., Shiratori, H., Mochida, K., Ikawa, Y., Saijoh, Y. and Hamada, H. (2001). The transcription factor FoxH1 (FAST) mediates Nodal signaling during anterior-posterior patterning and node formation in the mouse. *Genes Dev.* **15**, 1242-1256.

Yan, Y. T., Liu, J. J., Luo, Y., Chaosu, E., Haltiwanger, R. S., Abate-Shen, C. and Shen, M. M. (2002). Dual roles of Cripto as a ligand and coreceptor in the Nodal signaling pathway. *Mol. Cell. Biol.* **22**, 4439-4449.

Yeo, C. and Whitman, M. (2001). Nodal signals to Smads through Cripto-dependent and Cripto-independent mechanisms. *Mol. Cell* **7**, 949-957.

Yokota, C., Kofron, M., Zuck, M., Houston, D. W., Isaacs, H., Asashima, M., Wylie, C. C. and Heasman, J. (2003). A novel role for a nodal-related protein; Xnr3 regulates convergent extension movements via the FGF receptor. *Development* **130**, 2199-2212.

Zambrowicz, B. P., Imamoto, A., Fiering, S., Herzenberg, L. A., Kerr, W. G. and Soriano, P. (1997). Disruption of overlapping transcripts in the ROSA beta geo 26 gene trap strain leads to widespread expression of beta-galactosidase in mouse embryos and hematopoietic cells. *Proc. Natl. Acad. Sci. USA* **94**, 3789-3794.

Zhang, J., Talbot, W. S. and Schier, A. F. (1998). Positional cloning identifies zebrafish *one-eyed pinhead* as a permissive EGF-related ligand required during gastrulation. *Cell* **92**, 241-251.